Green Fluorescent Protein Variants as Ratiometric Dual Emission pH Sensors. 3. Temperature Dependence of Proton Transfer†

Tim B. McAnaney,‡ Xinghua Shi,‡ Paul Abbyad,‡ Henry Jung,‡ S. James Remington,§ and Steven G. Boxer*,‡

Department of Chemistry, Stanford University, Stanford, California 94305-5080, and Departments of Chemistry and Physics and Institute of Molecular Biology, University of Oregon, Eugene, Oregon 97403-1229

Received January 23, 2005; Revised Manuscript Received April 22, 2005

ABSTRACT: In parts 1 and 2 of this series [Hanson, G. T., McAnaney, T. B., Park, E. S., Rendell, M. E. P., Yarbrough, D. K., Chu, S. Y., Xi, L. X., Boxer, S. G., Montrose, M. H., and Remington, S. J. (2002) *Biochemistry 41,* 15477−15488; McAnaney, T. B., Park, E. S., Hanson, G. T., Remington, S. J., and Boxer, S. G. (2002) *Biochemistry 41,* 15489−15494], we described the structure, excited-state dynamics, and applications of pH-sensitive, ratiometric dual emission green fluorescent protein (deGFP) variants with fluorescence emission that is modulated between blue ($\lambda_{max} \cong 465$ nm) and green ($\lambda_{max} \cong 515$ nm) depending on the pH of the bulk solvent. In this paper, we consider the energetic origin of the dual emission properties of these GFP variants by examining the temperature dependence of the steady-state absorption and fluorescence emission. In most cases, the quantum yield of the green emission decreased as the temperature was lowered, indicating that the excited-state proton transfer (ESPT) which produces the green emitting form is an activated process. The activation energies of ESPT, determined by modeling the quantum yields of both blue and green emissions between 260 and 298 K in the context of a simple photocycle, were found to be larger at low pH than at high pH. These results indicate that the ratiometric dual emission properties of deGFP mutants are due to this pH-sensitive ESPT rate, combined with a modulation of the ground-state neutral and anionic chromophore populations with pH. The time-resolved fluorescence of one of the deGFP mutants was studied in detail. The time-resolved emission spectra of this mutant are the first ultrafast spectra obtained for a GFP. These spectra demonstrate that the rising kinetics for green emission, considered a hallmark of ESPT, is the sum of the contribution from both the neutral and intermediate anionic forms of the chromophore at the probe wavelength and may not be observed in all mutants that undergo ESPT, depending on the relative contributions of the two forms.

The green fluorescent protein (GFP)[1] from the jellyfish *Aequorea victoria* is widely used as a marker of gene expression and protein interaction within intact cells and organisms (*1*), and engineered variants of GFP have been used as physiological indicators and biosensors (*2*−*4*). The genetically encoded fluorescence of GFP is a result of an autocatalytic, post-translational cyclization and oxidation reaction of three consecutive amino acids to form the protein's chromophore. The high-resolution crystal structure (*5, 6*) shows an unusual 11-stranded β-barrel that shields the GFP chromophore from bulk solvent and creates a relatively rigid environment that is largely responsible for its high fluorescence quantum yield. The specific amino acid residues whose interactions further influence the spectroscopic properties of the chromophore line the inner surface of this β-barrel. Manipulation of the environment surrounding the chromophore has opened new opportunities to improve and manipulate various biochemical and spectroscopic properties of GFP, such as the sensitivity to pH (*3, 7*−*9*), redox potential (*10, 11*), metal (*12*−*14*) or halide concentration (*15*), quantum yields of fluorescence, and absorption or fluorescence maxima (*1, 16, 17*). In parts 1 and 2 of this series (*3, 18*), we described the structure, excited-state dynamics, and applications of pH-sensitive, ratiometric, dual emission GFP (deGFP) variants with fluorescence emission that is modulated between blue ($\lambda_{max} \cong 465$ nm) and green ($\lambda_{max} \cong 515$ nm) depending on the pH of the bulk solvent. In the following, we consider the energetic origin of the dual emission properties of these GFP variants by examining the temperature dependence of absorption and fluorescence emission.

Structural and spectroscopic studies of wild-type GFP indicate that the ground state of the chromophore exists in both neutral and anionic protonation states, denoted A and B, respectively, and a scheme describing the essential features

† This work was supported in part by grants from the NIH (GM27738 to S.G.B. and R01 GM42618 to S.J.R.). The fluorescence upconversion facilities are supported by the Medical Free Electron Laser Program of the Air Force Office of Scientific Research (Grant No. F49620-00-1-0349).

* To whom correspondence should be addressed. Tel: 650-723-4482. Fax: 650-723-4817. E-mail: sboxer@stanford.edu.

‡ Stanford University.

§ University of Oregon.

[1] Abbreviations: GFP, green fluorescent protein; ESPT, excited-state proton transfer; deGFP, dual emission green fluorescent protein; deGFP1, GFP variant (S65T/H148G/T203C); deGFP2, GFP variant (S65T/C48S/H148C); deGFP3, GFP variant (S65T/C48S/T203C); deGFP4, GFP variant (C48S/S65T/H148C/T203C); BFP, GFP variant (S65T/Y66H/Y145F) or blue fluorescent protein.

10.1021/bi050132a CCC: $30.25
Published on Web 05/25/2005

Scheme 1

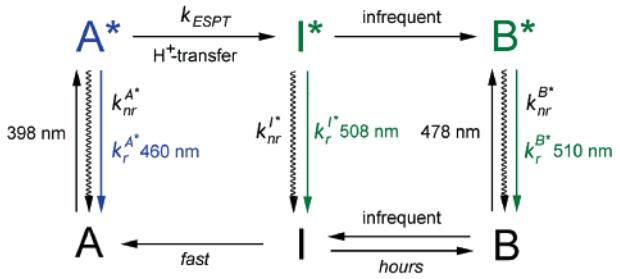

of its photochemistry and photophysics is shown (Scheme 1) (*19*). Excitation of either the neutral or anionic form of the chromophore results in green fluorescence at 510 nm from the anionic state. Direct excitation of the anionic chromophore B results in green emission with a high fluorescence quantum yield. Upon excitation of the neutral chromophore, A* rapidly converts to I*, a green-emitting form that appears to be similar to B*. However, I* (or I) rapidly re-forms A, while B is only formed to a very limited extent. The exact difference between B and I (or B* and I*) is not understood, but it has been suggested that structural relaxation of the protein may be required to convert I* and I into B. Time-resolved fluorescence studies have shown that the lack of appreciable steady-state emission from the excited state of the neutral chromophore can be attributed to an ultrafast, excited-state proton transfer (ESPT) reaction that quenches the blue emission and gives rise to the green-emitting anionic species (*19*). This was originally suggested since both the A* decay and I* rise in wild-type GFP are slowed upon deuteration of exchangeable protons. The minimal working model (*19*) in Scheme 1 provides a useful framework for describing GFP ground and excited-state dynamics (*18*), though we stress that it may not apply in detail to all GFP variants and ultimately oversimplifies the situation even for wild-type. The two-color emission from deGFPs has been attributed to an overall decrease in the rate of ESPT compared to wild-type so that appreciable A* emission can be seen at steady state, and structural work suggests that the difference is a result of different proton relay networks surrounding the chromophore (*3*). As with wild-type GFP, excitation of A in deGFPs leads very rapidly to a B-like species; however, B does not accumulate rapidly; therefore it is necessary to invoke a species such as I.

GFP-based biosensors that rely solely on excitation and emission from the anionic state suffer from the fact that it is often difficult to dissect whether in vivo changes in fluorescence intensity arise from changes in the concentration of the analyte being detected or the biosensor itself. Ratiometic GFP-based biosensors such as deGFPs and GFP FRET pairs (*12*), avoid many of these problems; however, to date, the quantum yield of blue fluorescence has always been limiting in cellular applications, even with the use of enhanced BFPs and CFPs (*20*, *21*). In this work, we explore the dramatic enhancement of blue fluorescence observed in deGFPs at low temperatures. We present temperature-dependent absorbance and fluorescence quantum yield measurements at acidic, neutral, and basic pH of four dual emission GFP variants: deGFP1 (S65T/H148G/T203C), deGFP2 (S65T/C48S/H148C), deGFP3 (S65T/C48S/T203C), and deGFP4 (S65T/C48S/H148C/T203C). The temperature dependence of the ground-state interconversion between the neutral and anionic states and the activation barriers for ESPT and nonradiative decay following excitation of the neutral chromophore are examined. These energetic features are crucial for understanding the ground- and excited-state proton-transfer reactions that underlie the spectroscopic properties of GFP and its mutants such as the low quantum yield of blue emission. In addition, we examine the time-resolved fluorescence of deGFP2 by fluorescence up-conversion spectroscopy to compliment previous studies on deGFP4 (*18*).

MATERIALS AND METHODS

Sample Preparation. Protein samples of the four deGFPs were prepared as described previously (*3*). It is noted that deGFP3 contains an additional mutation, C48S, that was not present when the protein was studied previously (*3*). This mutation was introduced to eliminate the possibility of a disulfide bridge at this surface-exposed site, and it is spectrally silent as shown by Hanson et al. in redox sensitive GFPs (roGFPs) (*10*). The protein samples were exchanged into three different 100 mM NaCl and 50 mM buffer solutions, at high, intermediate, and low pH, and one deuterated 100 mM NaCl and 50 mM buffer solution, at intermediate pD. The high-pH buffer was pH 9.2; the intermediate pH and pD buffers were chosen to correspond to the aqueous pK_a values measured for each mutant (*3*) and are listed in Table 1; the low-pH buffer was pH 5.6. deGFP1 showed a tendency to precipitate from solution at high concentrations at pH 5.6, so a pH 6.0 buffer was used instead for this mutant. Buffers used were MES, MOPS, HEPES, and Bis-Tris Propane as appropriate. For deuterated buffer solutions, the buffer was dissolved in D_2O and adjusted to the final pD using DCl or NaOD (buffers were corrected for the isotope effect on the pH meter (*22*)). Buffer exchange was performed by concentrating the protein followed by re-suspension in the desired buffer (repeated three times). A 60% (v/v) glycerol (or d_3-glycerol) solution was prepared in buffer containing the protein for subsequent temperature-dependent fluorescence and absorption studies.

Room-Temperature Quantum Yield Measurements. The quantum yields of emission following excitation at 400 nm were determined for the deGFPs in protonated glycerol/buffer solutions. Fluorescence spectra were recorded on a Spex fluorolog fluorimeter with a Spex 1620 dual-grating emission monochromator (Spex Industries, Metuchen, NJ) using a 10 mm path length cuvette and right-angle detection geometry. Fluorescence spectra were corrected for detection efficiency using a series of standards and technical emission spectra that covered the fluorescence range (*23*). The absorption spectrum of each sample was recorded on a Perkin-Elmer Lambda 12 UV/vis spectrophotometer (Perkin-Elmer, MA). Solutions were kept dilute ($A_{400} < 0.1$) to avoid inner filter effects. Solutions of 9-aminoacridine dissolved in water ($\lambda_{max,abs} = 400$ nm, $\Phi_F = 0.98$) were used as standards (*24*). Three separate solutions of the standard were prepared and measured, either at the beginning, middle, or end of acquiring the fluorescence spectra of the protein samples, to ensure no substantial instrument drift and to provide an estimate of the experimental error. These standard samples, normalized with respect to their absorption at the excitation wavelength, differed in their integrated intensity by no more than 6%. The quantum yield of fluorescence from the deGFPs was

calculated according to

$$\Phi_F^P = \frac{\int I_P(\lambda)\, d\lambda}{\int I_S(\lambda)\, d\lambda} \times \left(\frac{n_{glycerol/water}}{n_{water}}\right)^2 \times \frac{A_{400}^S}{A_{400}^P} \times \Phi_F^S \quad (1)$$

where $I_S(\lambda)$ and $I_P(\lambda)$ are the corrected emission spectra of the standard and protein solutions, A_{400}^S and A_{400}^P are the standard and protein absorptions at 400 nm, Φ_F^S is the standard's quantum yield of fluorescence, and the refractive indices n_{water} and $n_{glycerol/water}$ are fixed to their room temperature values of 1.33 and 1.42, respectively (*25*). The absorbance of samples was kept low such that eq 1 is applicable. In general, the fractions of absorbed light, that is, $1 - 10^{-A}$, should be used instead of absorbance. These room-temperature quantum yields were used to determine the temperature-dependent quantum yields described below.

Temperature-Dependent Fluorescence and Absorbance Measurements. The temperature-dependent fluorescence and absorption spectra of deGFPs in glycerol/buffer were collected using the same fluorimeter and spectrophotometer as used for the room-temperature quantum yield measurements. Variable temperature from 298 to 115 K was achieved using a miniature Joule-Thomson refrigerator (MMR Technologies, Mountain View, CA) and very thin (75 μm path length) sample geometry. For fluorescence measurements, samples were excited with 400 nm light and the resulting sample fluorescence was collected from 420 to 650 nm in a front-face geometry. Fluorescence and absorption spectra were taken in ~10 K intervals after cooling at a rate of ~0.1 K/s from the previous temperature point and a 3 min equilibration period at the desired temperature. A clear glass was obtained at 180 K and below if the sample was not equilibrated between 190 and 200 K. Measurements at 190 and 200 K, temperatures near the glass transition temperature (T_g), were not taken as the sample became opaque if maintained at these temperatures.

To determine the quantum yield of fluorescence as a function of temperature, variable temperature absorption spectra were first used to correct the fluorescence spectra for the change in sample absorption at the excitation wavelength. The ratio of the integrated fluorescence intensity relative to that at room temperature was then calculated and multiplied by the quantum yield of fluorescence measured at room temperature. The room-temperature quantum yield in deuterated glycerol/buffer solution was determined by normalizing the spectrum obtained in the Joule-Thomson refrigerator according to the pH-independent isosbestic point determined from the three spectra in protonated glycerol/buffer solution. The quantum yield of emission was further separated into the quantum yields from the different emitting states (A* and I*) by normalizing and subtracting the spectrum measured at low pH, which was typically dominated by A* emission. For deGFPs which had a substantial amount of I* emission even at low pH, a red-shifted spectrum of BFP was used to model the red edge of the A* emission spectrum.

Likewise, for the determination of the ground-state equilibrium constant, the integrated absorbances for each band (A and B) were determined from spectral decomposition, using the low-pH spectrum as a model. To remove from the spectrum the 280 nm protein band that partially obstructs the blue edge of the A band, the blue side of the 400 nm absorption band in the spectrum was fit to a log-normal line shape and extrapolated to 250 nm.

Fluorescence Upconversion Spectroscopy. The time-resolved fluorescence of deGFP2 at pH 6.0 and 9.2 in aqueous buffer was measured at 460 and 515 nm by a fluorescence upconversion setup described previously (*19*, *26*). Samples were excited by a 400 nm excitation pulse generated from the second harmonic of an argon ion-pumped titanium/sapphire laser. The instrument response function (IRF) generated from the mixing of the gate beam with scattered excitation light was typically ~160 fs, and the time window for data acquisition was 1.32 ns. The sample, stirred continuously in a 1-mm path length quartz cuvette, was excited at 82 MHz with 10 mW of light (12 pJ/pulse) polarized at the magic angle with respect to the gate beam. Time-resolved fluorescence spectra were obtained by tuning the phase matching angle for sum frequency generation in sync with the monochromator detection wavelength while at a fixed time delay (*27*). In practice, fine adjustments of the delay line were also required to compensate for the group velocity mismatch of the different spectral components traveling through the sample cuvette and the upconversion BBO crystal. A UG 11 filter provided good transmission of the upconverted light over the desired wavelength range while sufficiently blocking residual, scattered 400 nm excitation light. The spectrum recorded at $t = -1$ ps was subtracted from the spectra collected at positive time delays.

Data Analysis. Scheme 1, originally proposed for wild-GFP (*19*), was used as a model to analyze the temperature-dependent, ground-state equilibria and quantum yields of fluorescence. The equilibrium constant for ground-state interconversion, $A \rightleftharpoons B + H^+$, was determined according to

$$\ln K_{eq} = \ln\left(\frac{[B][H^+]}{[A]}\right) = \ln\left(\frac{\epsilon_A \int A^B(\lambda)\, d\lambda}{\epsilon_B \int A^A(\lambda)\, d\lambda}\right) - 2.3 \times pH \quad (2)$$

where $\int A^A(\lambda)\, d\lambda$ and $\int A^B(\lambda)\, d\lambda$ are the integrated absorbance of states A and B, and the ratio of extinction coefficients ϵ_A/ϵ_B is as determined from the ratio of the change of temperature-dependent integrated absorbance of B to that of A.

A van't Hoff plot of the natural logarithm of K_{eq} versus T^{-1} was used to determine the change in enthalpy associated with ground-state $A \rightleftharpoons B + H^+$ interconversion. The data near room temperature (298−260 K) were fit to the integrated form of the van't Hoff equation (*28*, *29*)

$$\ln \frac{K_{eq}}{K_0} = \frac{\Delta H_0 - T_0 \Delta C_p}{R}\left(\frac{1}{T_0} - \frac{1}{T}\right) + \frac{\Delta C_p}{R} \ln \frac{T}{T_0} \quad (3)$$

where ΔC_P is change in heat capacity, assumed to be temperature independent over the range of temperatures, T_0 is the reference temperature of 298K, and K_0 and ΔH_0 are the equilibrium constant and enthalpy, respectively, at T_0.

To model the excited-state dynamics of the deGFPs, both A* and I* were assumed to have individual radiative (k_r) and nonradiative (k_{nr}) decay rates and were connected via the rate of ESPT (k_{ESPT}). The expressions for the quantum

yields of fluorescence from A* and I* can be derived as

$$\Phi_F^A = \frac{k_r^{A^*}}{k_r^{A^*} + k_{nr}^{A^*} + k_{ESPT}} = \frac{1}{1 + k'^{A^*}_{nr} + k'_{ESPT}} \quad (4)$$

$$\Phi_F^I = \frac{k_r^{I^*} k_{ESPT}}{(k_r^{A^*} + k_{nr}^{A^*} + k_{ESPT})(k_r^{I^*} + k_{nr}^{I^*})} = \frac{k'_{ESPT}}{(1 + k'^{A^*}_{nr} + k'_{ESPT})(1 + k'^{I^*}_{nr})} \quad (5)$$

where the latter expressions give the nonradiative rates relative to the radiative rates of the precursor state. To model the temperature dependence, the nonradiative decay rates, including the rate of excited-state proton transfer, were modeled according to the Arrhenius expression

$$k'_i = A'_i e^{-E_i/RT} \quad (6)$$

where A'_i is the Arrhenius preexponential factor, E_i is the activation energy, R is the gas constant, and T is the absolute temperature. This yields two functions $\Phi_F^A(T, A'^{A^*}_{nr}, E_{nr}^{A^*}, A'_{ESPT}, E_{ESPT})$ and $\Phi_F^I(T, A'^{A^*}_{nr}, E_{nr}^{A^*}, A'_{ESPT}, E_{ESPT}, A'^{I^*}_{nr}, E_{nr}^{I^*})$ which were simultaneously fit to the data. In all cases studied, the best fit to the data had $k'^{I^*}_r > k'^{I^*}_{nr}$ and could therefore be equally well-fit by the simplified functions $\Phi_F^A(T, A'^{A^*}_{nr}, E_{nr}^{A^*}, A'_{ESPT}, E_{ESPT})$ and $\Phi_F^I(T, A'^{A^*}_{nr}, E_{nr}^{A^*}, A'_{ESPT}, E_{ESPT})$ where I* decayed solely by $k'^{I^*}_r$.

RESULTS

Room-Temperature Quantum Yields. The total quantum yield of emission (Φ_F) for each deGFP varies dramatically as a function of pH. At low pH, Φ_F varies from ~0.02 to 0.08 depending on the mutant, whereas at high pH, Φ_F is much higher, varying from 0.22 to 0.44. Breaking down Φ_F into the individual contributions from the A* and I* states (Φ_F^A and Φ_F^I, respectively) reveals two distinct classes of behavior for the deGFPs (Table 1). For deGFP3 and -4, Φ_F^A increases as the pH is lowered, whereas for deGFP1 and -2, Φ_F^A is relatively *insensitive* to pH. All four mutants show a decrease in Φ_F^I upon lowering the pH. Deuteration of exchangeable protons at intermediate pD leads to emission spectra similar to that observed at low pH. The interesting behavior of Φ_F^A in deGFP1 and -2 led us to further characterize the excited-state dynamics of deGFP2 by fluorescence upconversion spectroscopy (the dynamics of deGFP4 were characterized in earlier work (*18*)).

Temperature Dependence of Absorption. Qualitatively, for all of the deGFPs studied, as the temperature is lowered from 298 to 210 K, the integrated area of the absorption band of the neutral chromophore (A) increases while that of the anionic chromophore (B) decreases as determined from the integrated absorption bands of each species. At low pH, the population of the anionic chromophore at room temperature is close to zero and the increase in absorbance of the neutral chromophore upon lowering the temperature is modest (~10−15%). For intermediate and high pHs, where the room temperature populations of the anionic chromophore are more substantial, the absorption band of the neutral chromophore increases more dramatically (up to 75%) as the equilibrium shifts toward the neutral chromophore at lower temperatures. At 180 K and below, the intensities of the A and B absorption bands remain approximately constant, and the predominant effect of lowering the temperature further is a narrowing of the bands and a sharpening of vibronic structure. A typical series of temperature-dependent absorption spectra are shown in Figure 1A,C,E for deGFP1 at pH 6.00, 8.02, and 9.20 (also see Figure 1A in ref *3*). deGFP2 shows a slight deviation from the behavior of the other variants at intermediate and high pH. The ratio of the integrated absorption bands (A/B) increases from room temperature until ~260−270 K, then decreases until 230 K, and then resumes increasing again at lower temperatures.

A van't Hoff plot of the natural logarithm of K_{eq} (eq 2) versus T^{-1} was used to determine the change in enthalpy associated with ground-state $A \rightleftharpoons B + H^+$ interconversion (Figure 2). Although the slopes of the van't Hoff plot of deGFPs 1, 3, and 4 did not exhibit the change in sign seen in deGFP2, an abrupt decrease in the slope below ~260 K is observed in all of the mutants. Fitting the data close to room temperature (298−260 K) to eq 3, where the heat capacity change is assumed constant over the narrow temperature range, yields the thermodynamic parameter ΔH° listed in Table 1. The vertical displacements on the van't Hoff plot indicate that K_{eq}, and therefore the free energy of the reaction, changes with pH. This is different from simple acid−base reactions where K_{eq} would be constant at different pHs. The change of K_{eq} for deGFPs can be due to different protein conformations induced by changes in pH, as observed in the deGFP1 crystal structure (*3*).

Temperature Dependence of Steady-State Fluorescence. Following excitation of the neutral chromophore at 400 nm, the four deGFPs exhibit spectra characteristic of emission from the excited states of both the neutral (A*, ~460 nm) and anionic (I*, ~515 nm) chromophores, with relative intensities that depend on pH and temperature (see Figure 1B,D,F and also Figure 1C in ref *3*). As the temperature is lowered, Φ_F^A increases dramatically for all deGFP variants studied, regardless of pH. At low pH and intermediate pD, emission from I* is either absent at room temperature or disappears 40−60 K below room temperature, depending on the mutant. At intermediate and high pH, emission from I* dominates the room-temperature fluorescence spectrum but decreases in intensity as the temperature is lowered to 210 K. At 180 K and below, the intensity of emission from I* is generally constant if it remains present in the spectrum at all. Only deGFP1 shows behavior that did not fit this description. For this mutant at high pH, Φ_F^I decreases from room temperature to 250 K and then exhibits a large increase in intensity (>150%) followed by a decrease between 180 and 115 K. At intermediate pH, Φ_F^I shows the same general trend, although the increase in intensity is less dramatic and Φ_F^I below 180 K is fairly constant, showing only a slight increase over the low-temperature range. The temperature dependences of Φ_F^A and Φ_F^I are summarized in Figure 3 for the four deGFP variants.

It is difficult to fit eqs 4−6 to the temperature dependence of the fluorescence quantum yields over the entire temperature range above T_g; however, modeling the behavior of the deGFPs with an Arrhenius expression for the nonradiative rates over the temperature range of 260−298 K yields the

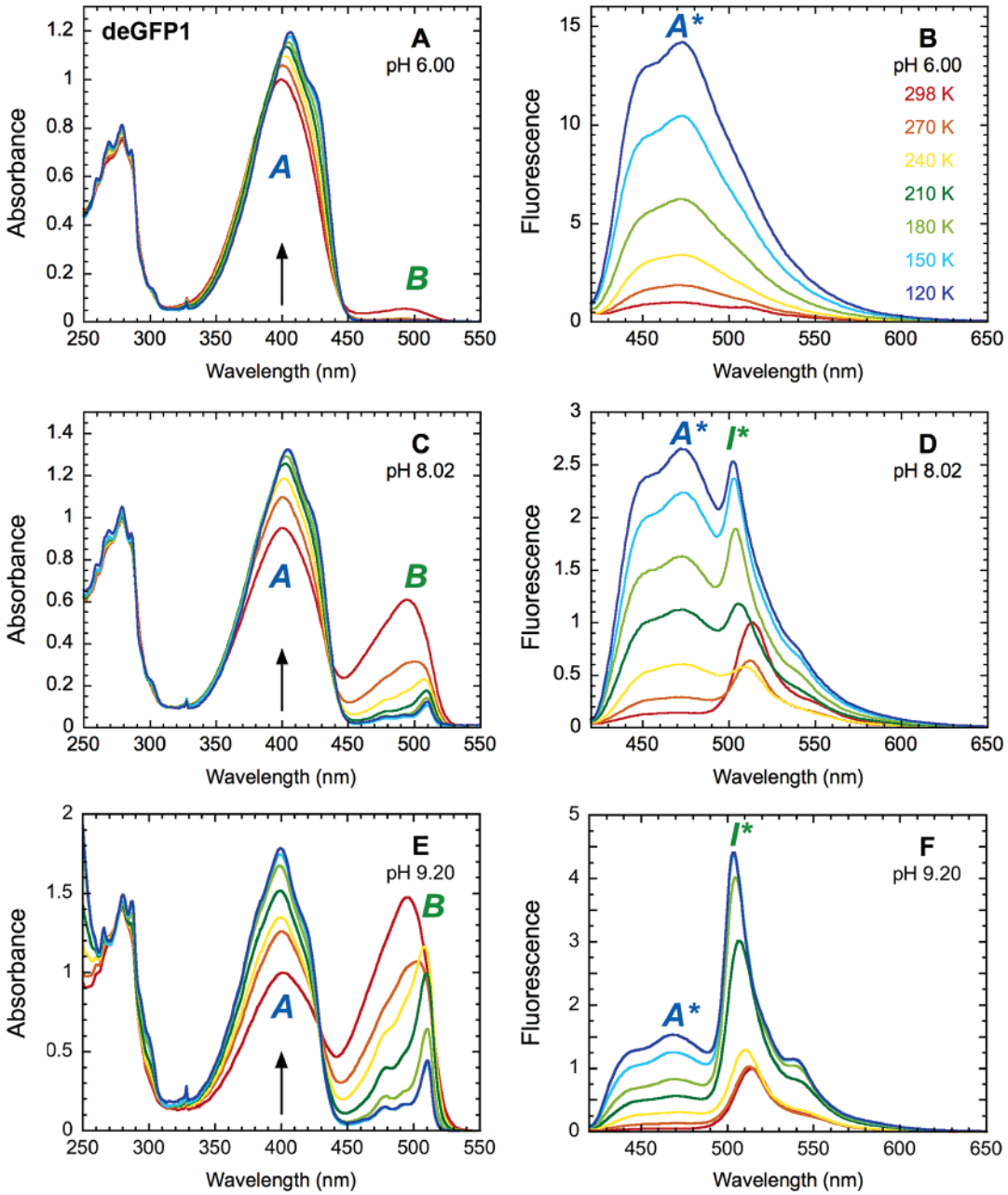

FIGURE 1: Steady-state absorbance and fluorescence spectra of deGFP1 from 298 K (red) to 120 K (blue) in ~30 K intervals. Absorbance (A) and fluorescence (B) at pH 6.00. Absorbance (C) and fluorescence (D) at pH 8.02. Absorbance (E) and fluorescence (F) at pH 9.20. The excitation wavelength for fluorescence measurements, 400 nm, is indicated by the arrows in the absorbance plots. Both absorbance and fluorescence spectra were normalized to the peak value of the spectrum at 298 K. Fluorescence intensities were corrected for the change in absorbance with temperature at the excitation wavelength.

activation energies listed in Table 1. For all mutants, the nonradiative decay rate is generally small compared with the radiative rate of I*, and the data can also be adequately modeled with a simplified scheme where I* primarily decays radiatively ($k_r^I > k_{nr}^I$). This implies that the intrinsic quantum yield of emission from I*, once formed via proton transfer, is quite high (i.e., $\Phi_F^I/\Phi_{ESPT} \sim 1$) and that emission from I* serves as a direct reporter of excited-state proton transfer. It should be noted that the kinetic model presented here is not capable of producing a minimum in the function $\Phi_F^A(T)/\Phi_F^I(T)$ as is observed with deGFP1.

Room-Temperature Time-Resolved Fluorescence of deGFP2. The time-resolved fluorescence decays of deGFP2 at 460 and 515 nm were recorded at low and high pH (Figure 5). In addition, discrete time-resolved emission spectra were recorded at different delay times following excitation of the neutral chromophore (Figure 6). Two separate fluorescence bands at ~460 and 515 nm, analogous to those seen at steady state, are readily visible in the time-resolved emission spectra. The low-pH emission spectra are dominated by emission from A* at 460 nm with a small, secondary peak from I* appearing at ~515 nm. At high pH, the A* emission dominates the spectrum at early times and appears to decay in a manner similar to that observed at low pH. Emission from I* at 515 nm, however, rises to its maximum intensity in ~100 ps and subsequently decays on the nanosecond time scale. The time-resolved emission spectra clearly demonstrate that the dynamics measured at 460 nm can be attributed to a single decaying species, A*, whereas the dynamics measured at 515 nm are the sum of the individual kinetics

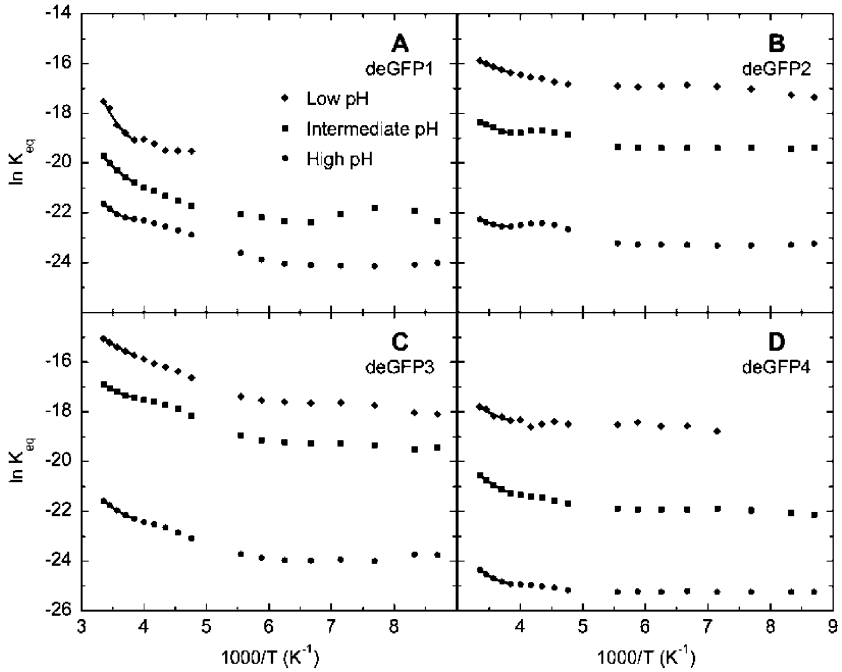

FIGURE 2: van't Hoff plot of the natural logarithm of K_{eq} vs T^{-1} for deGFP1 (A) deGFP2 (B), deGFP3 (C), and deGFP4 (D). Measurements were done at low pH (diamonds), an intermediate pH (squares), and at high pH (circles) as described in the text. Fits to the integrated form of the van't Hoff equation between 298 and 260 K are shown. Measurements in deuterated buffer have been omitted for clarity.

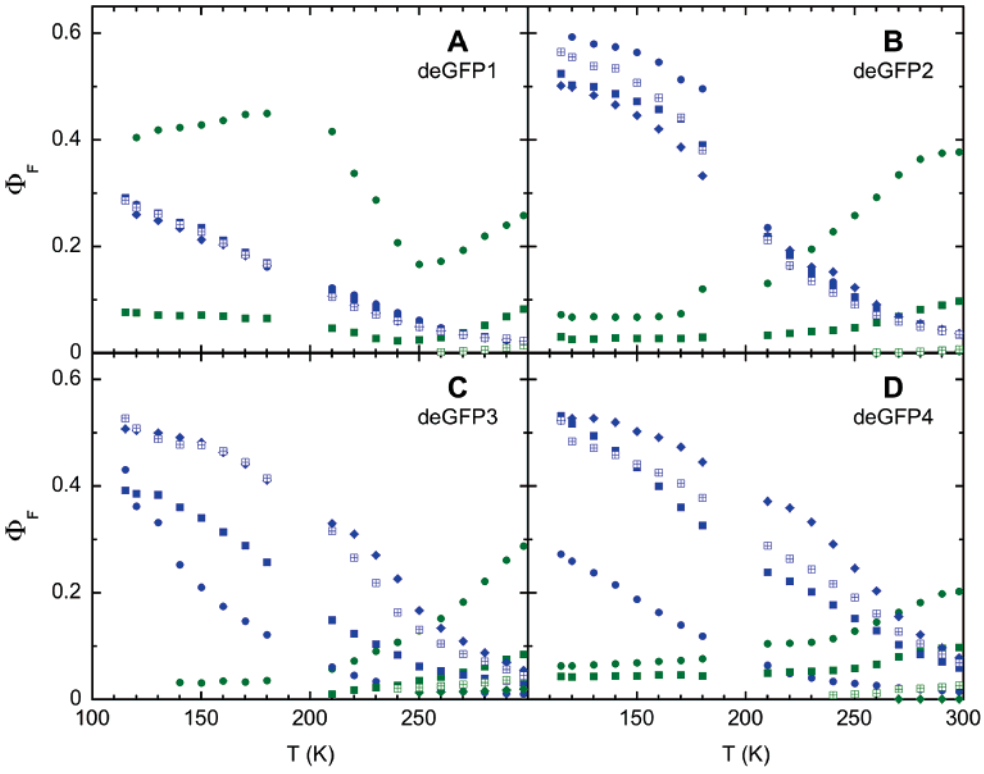

FIGURE 3: Quantum yields of fluorescence from A* (blue) and I* (green) as a function of pH and temperature for (A) deGFP1, (B) deGFP2, (C) deGFP3, and (D) deGFP4. Measurements were done at low pH (diamonds), an intermediate pH (squares), and at high pH (circles) as described in the text. Measurements at intermediate pD (open squares with cross) are also shown.

from two species with overlapping emission bands, A* and I*. Therefore, to isolate the emission at 515 nm coming solely from I*, the A* dynamics measured at 460 nm are normalized to the initial ($t = 0$) emission amplitude at 515 nm and subtracted from the data, since the early-time emission at 515 nm (<1 ps) can be attributed primarily to A* decay. The resulting kinetic trace reflects purely the I* emission dynamics in deGFP2 (Figure 5, lower panels).

DISCUSSION

Ground-State Equilibria of deGFPs. The ground state of the wild-type GFP chromophore exists in both neutral and anionic forms, which absorb at 398 (band A) and 478 (band B) nm, respectively. Although in wild-type the ratio of the two forms is largely independent of pH or ionic strength, in mutants of GFP, the ratio often shows an increased sensitivity

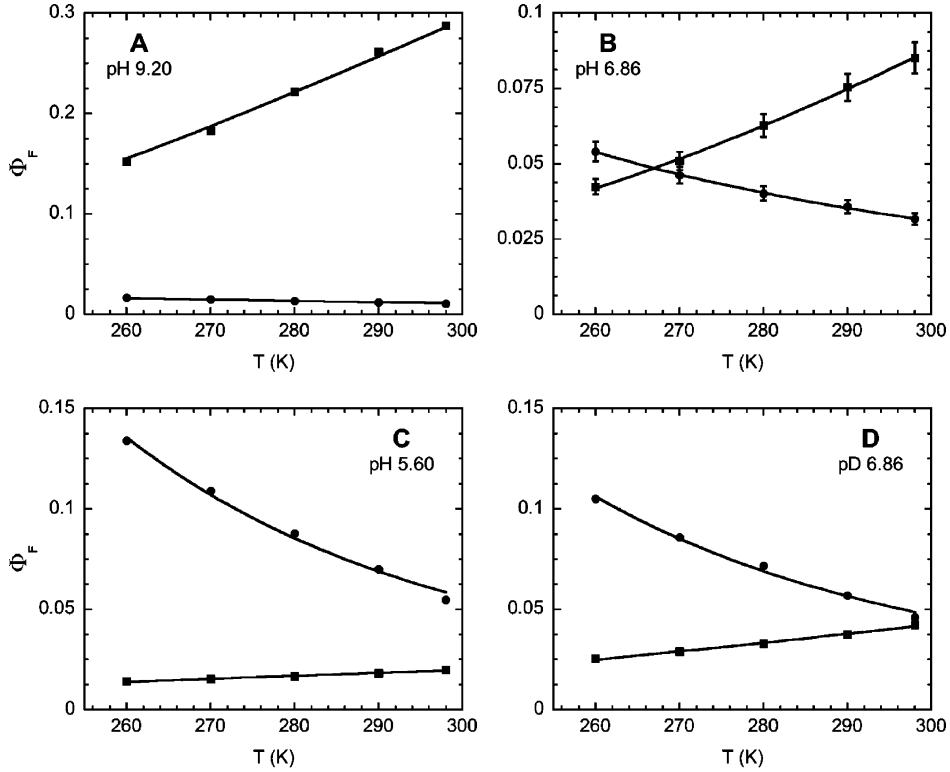

FIGURE 4: Simultaneous fits to eqs 4 and 5 of Φ_F^A (circles) and Φ_F^I (squares) for deGFP3 from 298 to 260 K at high (A), intermediate (B), and low (C) pH and intermediate pD (D). The fits are derived from the kinetics imposed by Scheme 1 assuming an Arrhenius temperature dependence of k_{ESPT} and k_{nr}^{A*}. Error bars depicted in (B) are estimates based on repeated measurements of 9-aminoacridine standards as described in the text. The fit results are summarized in Table 1.

Table 1: Spectroscopic Parameters Derived from Temperature-Dependent Absorbance and Fluorescence Measurements of deGFPs

	$\Delta H°$ (kJ/mol)[a]	Φ_F^I 298 K[b]	Φ_F^A 298 K[b]	E_{ESPT} (kJ/mol)[c]	E_{nr}^A (kJ/mol)[c]
		deGFP1			
pH 9.20	21 ± 1	0.26	0.021	18 ± 1	11 ± 1
pH 8.02	25 ± 2	0.08	0.023	24 ± 1	7 ± 1
pD 8.02	35 ± 2	0.015	0.024	25 ± 5	9 ± 1
pH 6.00	44 ± 8	0.001	0.022	-	11 ± 1
		deGFP2			
pH 9.20	11 ± 1	0.40	0.036	19 ± 4	14 ± 4
pH 7.25	12 ± 3	0.10	0.035	23 ± 1	14 ± 1
pD 7.25	12 ± 1	0.007	0.036	31 ± 4	10 ± 1
pH 5.60	10 ± 1	0.005	0.038	32 ± 10	14 ± 1
		deGFP3			
pH 9.20	17 ± 1	0.29	0.011	16 ± 3	3 ± 2
pH 6.86	13 ± 1	0.085	0.032	21 ± 1	9 ± 1
pD 6.86	13 ± 1	0.042	0.045	22 ± 1	14 ± 1
pH 5.60	13 ± 1	0.020	0.055	20 ± 3	16 ± 1
		deGFP4			
pH 9.20	16 ± 1	0.20	0.015	15 ± 1	8 ± 1
pH 7.37	19 ± 1	0.10	0.059	19 ± 1	14 ± 1
pD 7.37	13 ± 3	0.026	0.069	24 ± 8	15 ± 1
pH 5.60	17 ± 5	0.001	0.078	27 ± 10	18 ± 1

[a] Ground-state enthalpy change determined by fitting the absorbance data near room temperature to the integrated form of van't Hoff equation (eq 3). [b] Room-temperature quantum yields of emission determined by decomposing the fluorescence spectra into individual A* and I* emission bands. The error is less than 6%. [c] Activation energies determined by fitting the quantum yields of emission near room temperature to eqs 4 and 5.

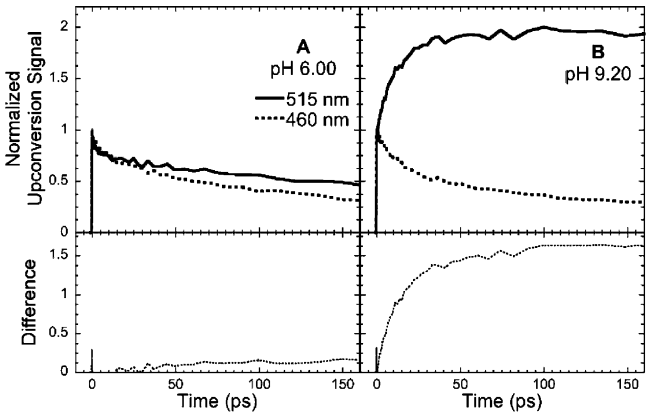

FIGURE 5: Room-temperature fluorescence upconversion measurements of deGFP2. The time-resolved emission measured at 460 nm (dashed line) and 515 nm (solid line) at pH 6.00 (A) and 9.20 (B). The kinetics have been normalized to the instantaneous emission at $t = 0$ ps. The kinetic trace below each panel is the difference in the normalized kinetics measured at the two wavelengths (515−460 nm).

to these and other properties of the surrounding medium (*7*, *30*). The ground-state equilibria of the deGFPs described here show a strong dependence on both pH and temperature. In this work, we determined the standard reaction enthalpy for the ground-state interconversion process from the temperature dependence of the equilibrium constant. Near room temperature, all of the deGFPs exhibit a negative slope associated with $A \rightleftharpoons B + H^+$ interconversion indicating that the neutral state of the chromophore is the enthalpically preferred state (Figure 2). With the exception of deGFP1, $\Delta H°$ is approximately independent of pH, and differences in the equilibrium constant (vertical displacements on the van't Hoff plot) can be attributed to pH-dependent changes in $\Delta S°$, through $-RT \ln K_{eq} = \Delta H° - T\Delta S°$. These vertical displace-

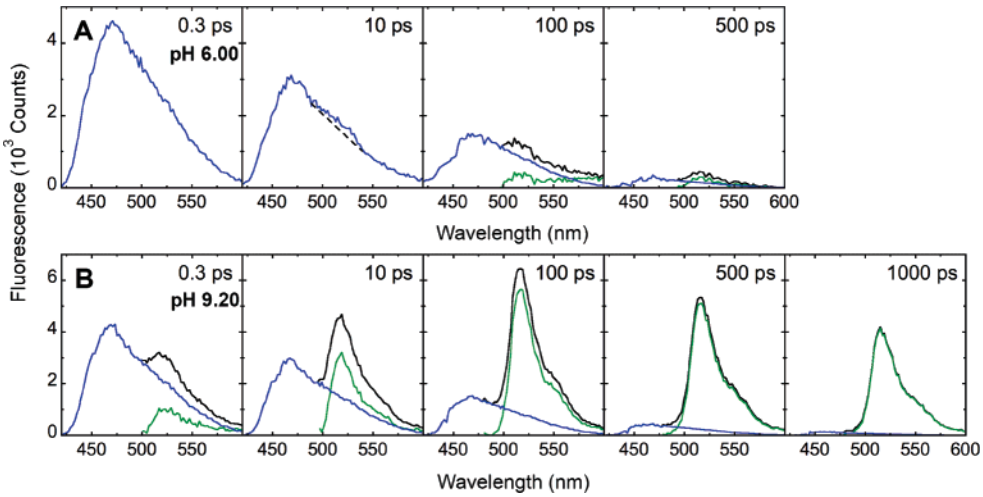

FIGURE 6: Room temperature time-resolved emission spectra of deGFP2 at $t = 0.300$, 10, 100, 500, and 1000 ps at pH 6.00 (A) and 9.20 (B). The $t = 1000$ ps spectrum is shown only for pH 9.20. The spectrum at $t = 0.3$ ps at pH 6.00 was used as a model of pure A* emission to decompose the spectra into contributions from A* (blue) and I* (green).

ments indicate that the change in entropy at low pH is greater than at high pH by ~40−60 J/mol·K, with deGFP1 showing the smallest change in $\Delta S°$ across the pH range.

For deGFP1, $\Delta H°$ changes from 21 to 44 kJ/mol as the pH is lowered. This change in $\Delta H°$ can be related to the crystal structure at low and high pH. Except for minor rearrangements, the low-pH structure (*3*) is superimposable on the S65T GFP structure solved at low and high pH (*7*), while the high-pH structure (*3*) reveals a large structural change of the β-barrel topology, specifically a twisting and displacement of the β-strand containing residues 143−150. At high pH, Ser147 moves from its normally solvent-exposed location to an interior location where it can form a hydrogen bond with the phenolate oxygen. At low pH, the hydrogen bond capabilities of the phenol oxygen are restricted and consequently, the sequestering of Ser147 is not energetically favorable (see Figures 3 and 4 of ref *3*). These structural changes lead to the changes observed in $\Delta H°$. The neutral state is enthalpically more favored in the low-pH conformation ($\Delta H° = 44$ kJ/mol) than in the high-pH conformation ($\Delta H° = 21$ kJ/mol). So far, only the crystal structure of deGFP1 has been determined (*3*). Other mutants in this series may share these pH-dependent structural properties, and crystal structures of those mutants will be solved to test this hypothesis.

As the temperature is lowered to ~250 K, the slope of the van't Hoff plot changes and becomes more shallow, with deGFP2 exhibiting an extreme case where the slope changes sign over a small temperature range. The observed curvature of the van't Hoff plot may be due to a nonzero heat capacity change or a more complex energy landscape than is reflected by a simple $A \rightleftharpoons B + H^+$ interconversion scheme. Hole-burning experiments have demonstrated that the ground state of the intermediate anionic state I is stable and populated at low temperatures (*31*−*33*), and more recent work has shown that it can be stabilized at room temperature by mutagenesis (*34*). The absorption band of the I state is reported to lie at ~500 nm at room temperature; therefore, it is possible that the red shift observed for the anionic band upon lowering the temperature (for example, ~494 → 510 nm for deGFP1, Figure 1C) represents B ↔ I interconversion. Regardless of the exact nature of the state being formed, it remains plausible that temperature-dependent changes in the surrounding protein structure cause other subpopulations to become populated at lower temperatures. The inability of Scheme 1 to quantitatively explain the temperature dependence of Φ_F^I and Φ_F^A down to T_g, as well as the inability to explain the dramatic increase in Φ_F^I observed for deGFP1 at ~250 K, points to the existence of a more complicated ground-state (and potentially excited-state) energy landscape at lower temperatures.

Activated Excited-State Proton Transfer. Green fluorescence is observed almost exclusively in the steady state down to ~77 K following excitation of the neutral chromophore in wild-type GFP. Indeed, to obtain significant amounts of blue emission (460/510 nm peak emission intensity > 1/4), wild-type GFP must either have its exchangeable hydrogens replaced with deuterons and the temperature lowered to 77 K (*19*) or, if fully protonated, the temperature must be further lowered to ~4 K (*34*). These observations suggest that the ultrafast excited-state proton transfer in wild-type is an almost activationless process. In contrast to wild-type GFP, the deGFP mutants studied here show evidence for an activated ESPT process. For most chromophores, the quantum yield of emission from the excited-state increases as the temperature is decreased because competing nonradiative decay pathways, such as internal conversion to the ground state, are suppressed. This is true of model compounds of the GFP chromophore (*35*−*38*), BFP (*39*), and the neutral chromophore of the deGFPs studied here at low pH (Figure 1B). Upon excitation of the neutral state, the intensity of emission from the anionic state of deGFPs decreases noticeably as the temperature is lowered, providing strong evidence that the emitting species is formed via an activated process. This observation, in conjunction with the dramatic isotope effect on the ratio of blue/green emission, indicates that an activated excited-state proton-transfer reaction connects the A* and I* excited states.

Modeling the behavior of Φ_F^A and Φ_F^I in the high-temperature range according to Scheme 1 reveals a pH-dependent modulation of the activation energy and, therefore, rate of ESPT (Table 1). All of the deGFPs show a greater activation energy for ESPT at low pH than at higher pH;

replacing exchangeable hydrogens with deuterons generally raises the activation energy compared to the corresponding activation energy in protonated buffer. At low pH, the rate of proton transfer in deGFP1 is so slow that almost no I* emission is observed at steady state following excitation of A (Figure 1B); therefore, it is not possible to determine an activation energy at this pH. The activation energy of ESPT is seen to vary from ~15 to 30 kJ/mol depending on the variant and the bulk pH.

The excited-state proton-transfer reaction competes against one or more nonradiative decay pathways from the excited state of the neutral chromophore back to the ground state. The existence of at least one activated, nonradiative decay pathway is evident at low pH where there is relatively little ESPT, and therefore little or no emission from I*, but still a dramatic enhancement of Φ_F^A with decreasing temperature. Whether or not the activation energy of this competing nonradiative decay pathway is also pH dependent appears to depend on the particular mutant; however, in all cases, $E_{nr}^{A^*}$ is smaller than E_{ESPT}. The origin of dual-emission, therefore, appears to be a balance of the relative rates of ESPT and nonradiative decay by modulating the activation energy of these excited-state decay pathways. Interestingly, for deGFP3 and -4, where $E_{nr}^{A^*}$ also appears to be dependent on pH, the activation energies follow the same trend as that observed for E_{ESPT}, suggesting that the same factors, presumably structural, that favor ESPT also favor nonradiative decay back to the ground state.

*The Dominant Decay Pathway of A**. The protein environment of wild-type GFP provides an optimal environment for excited-state proton transfer, making it an essentially activationless process. This results in an ultrafast rate of ESPT that dominates the decay kinetics of A* emission (i.e., $k_{ESPT} \gg k_{nr}^{A^*}$) (*19*). Thus, green light is exclusively emitted at all temperatures sampled by the organism, when energy transfer from aequorin to the blue A state occurs. In previous work, we showed that the decay of A* in deGFP4 is dependent on pH (*18*). The rapid decay of A* emission at high pH was attributed to ESPT, although the process is not as fast as that observed in wild type; consequently, some blue light is also emitted. The relatively modest kinetic isotope effect observed at high pH implies that the rates of ESPT and nonradiative decay to the ground state are comparable (i.e., $k_{ESPT} \approx k_{nr}^{A^*}$). At low pH, the lifetime of A* increases substantially, indicating that the rate of ESPT has slowed, and the lack of a kinetic isotope effect indicates that the decay of A* is no longer dominated by ESPT ($k_{ESPT} \ll k_{nr}^{A^*}$). The observation of a pH-dependent Φ_F^A for deGFP4 and -3 is consistent with earlier conclusions based upon experiments on deGFP4 and indicates that deGFP3 likely operates by a similar mechanism. The room-temperature rates extracted from modeling the temperature-dependent data for deGFP3 and -4 further confirm that, at low pH, $k_{ESPT} \ll k_{nr}^{A^*}$ and that, at high pH, $k_{nr}^{A^*}$ are roughly 2−3 times faster than k_{ESPT}. Unlike wild-type GFP, in deGFP3 and -4, nonradiative decay is the dominant mechanism for A* decay at most pHs; however, at high pH, the rate of ESPT becomes comparable.

The observation that the room temperature Φ_F^A is relatively insensitive to pH for deGFP1 and -2 suggests that ESPT is unlikely to be the dominant mechanism for A* decay at any pH. Despite being slowed, the rate of ESPT is not negligible, and emission from I* is readily observed at high pH due largely to the high quantum yield of emission from I* once formed. These results also indicate that the opposing changes in the blue and green emission intensities that make deGFPs useful as biological pH sensors are due both to the modulation of the rate of ESPT, which has a large impact on the intensity of I* emission, and the ground-state A to B ratio, which scales the A* emission according to the ground-state population of A.

Time-Resolved Fluorescence Kinetics and Spectra of deGFP2. To further investigate the relative insensitivity of Φ_F^A to changes in pH exhibited by deGFP1 and -2, the time-resolved kinetics of deGFP2 at room temperature were examined by fluorescence upconversion spectroscopy. The monoexponential kinetics inherent in Scheme 1 dictate that, if Φ_F^A remains constant as the pH is changed, the decay of A* must also remain unchanged. In the case of wild-type GFP or its mutants including the deGFPs, the observed decay of A* emission exhibits heterogeneous kinetics. For heterogeneous kinetics, an identical quantum yield can also be due to compensating changes in a multiexponential decay. Therefore, to distinguish between these two possibilities, the decay of A* was measured at 460 nm. As seen in Figure 5, the decay of A* is almost identical at high and low pH despite exhibiting heterogeneous kinetics, and this gives rise to the relatively constant Φ_F^A measured at steady state. It is therefore likely that the rate of nonradiative decay of A* dominates at both high and low pH.

Although the rate of ESPT does not dominate the decay kinetics of A*, the overall yield of proton transfer is directly proportional to k_{ESPT} and therefore has a substantial effect on the *amplitude* of I* emission measured at 515 nm. The conclusions from previous measurements of the time-resolved emission of deGFP4 at 460 and 515 nm relied on an analysis that assumed the kinetics probed at 515 nm were a sum of the kinetics of both the A* and I* states. The time-resolved spectra of deGFP2 at low pH (Figure 6A) clearly demonstrate that the line shape of the emission band from the neutral chromophore is quite broad and extends beyond 515 nm, even on the ultrafast time scale. At high pH (Figure 6B), the time-resolved spectrum at 300 fs indicates that almost all of the instantaneous (IRF-limited) intensity observed at 515 nm can be attributed to the A* state and is not a result of direct excitation of the blue edge of the B band and subsequent emission from B*. A quantitative analysis of the rising kinetics of I*, whether in deGFPs, wild-type, or other variants, likely requires subtraction of the A* dynamics measured at 460 nm, normalized to the instantaneous emission intensity observed at 515 nm. These difference traces for deGFP2 are shown in the lower panels of Figure 5 and represent the kinetics and relative amplitude of I* emission. As expected, lowering the pH dramatically decreases the yield of proton transfer and reduces the amplitude of I* emission compared to that observed at high pH.

Conclusions. The results presented here suggest that the dual-emission behavior of deGFPs is a result of both a pH-sensitive ground-state equilibrium and a pH-dependent modulation of the rate of ESPT. In general, the activation energy for ESPT is dependent on the pH of the surrounding

medium and is likely the result of pH-dependent structural changes in the vicinity of the chromophore. In contrast to wild-type GFP, the activation energy of ESPT in deGFPs slows down the overall rate of ESPT such that it is comparable to, or substantially slower than, competing nonradiative decay channels back to the ground state. Further structural characterization of the factors that appear to simultaneously suppress ESPT and nonradiative decay back to the ground state in deGFP3 and -4 may provide insights into the rational design of improved deGFPs with higher quantum yields of blue emission. The temperature dependence of the quantum yields of emission are well-described by a simple photocycle, summarized in Scheme 1, near room temperature; however, at temperatures below ~250 K, other conformations of the protein appear to be stable and complicate the observed dynamics. Finally, ultrafast time-resolved measurements of deGFP2 suggest that the detection of rising kinetics for I* emission, considered a characteristic signature of ESPT, is a function of the relative amplitudes of A* and I* emission at the probe wavelength and may not be observed in all systems that undergo ESPT.

ACKNOWLEDGMENT

The authors wish to thank Karen Kallio for helpful advice and discussion. X.S. acknowledges a William R. and Sara Hart Kimball Stanford Graduate Fellowship. P.A. acknowledges financial support from the Fonds de recherche sur la nature et les technologies and the National Science and Engineering Research Council of Canada.

REFERENCES

1. Tsien, R. Y. (1998) The green fluorescent protein, *Annu. Rev. Biochem. 67*, 509−544.
2. Truong, K., Sawano, A., Mizuno, H., Hama, H., Tong, K. I., Mal, T. K., Miyawaki, A., and Ikura, M. (2001) FRET-based in vivo Ca2+ imaging by a new calmodulin-GFP fusion molecule, *Nat. Struct. Biol. 8*, 1069−1073.
3. Hanson, G. T., McAnaney, T. B., Park, E. S., Rendell, M. E. P., Yarbrough, D. K., Chu, S. Y., Xi, L. X., Boxer, S. G., Montrose, M. H., and Remington, S. J. (2002) Green fluorescent protein variants as ratiometric dual emission pH sensors. 1. Structural characterization and preliminary application, *Biochemistry 41*, 15477−15488.
4. Miyawaki, A. (2003) Fluorescence imaging of physiological activity in complex systems using GFP-based probes, *Curr. Opin. Neurobiol. 13*, 591−596.
5. Ormö, M., Cubitt, A. B., Kallio, K., Gross, L. A., Tsien, R. Y., and Remington, S. J. (1996) Crystal structure of the *Aequorea victoria* green fluorescent protein, *Science 273*, 1392−1395.
6. Yang, F., Moss, L. G., and Phillips, G. N. (1996) The molecular structure of green fluorescent protein, *Nat. Biotechnol. 14*, 1246−1251.
7. Elsliger, M. A., Wachter, R. M., Hanson, G. T., Kallio, K., and Remington, S. J. (1999) Structural and spectral response of green fluorescent protein variants to changes in pH, *Biochemistry 38*, 5296−5301.
8. Kneen, M., Farinas, J., Li, Y. X., and Verkman, A. S. (1998) Green fluorescent protein as a non-invasive intracellular pH indicator, *Biophys. J. 74*, A181−A181.
9. Miesenbock, G., DeAngelis, D. A., and Rothman, J. E. (1998) Visualizing secretion and synaptic transmission with pH-sensitive green fluorescent proteins, *Nature 394*, 192−195.
10. Hanson, G. T., Aggeler, R., Oglesbee, D., Cannon, M., Capaldi, R. A., Tsien, R. Y., and Remington, S. J. (2004) Investigating mitochondrial redox potential with redox-sensitive green fluorescent protein indicators, *J. Biol. Chem. 279*, 13044−13053.
11. Ostergaard, H., Henriksen, A., Hansen, F. G., and Winther, J. R. (2001) Shedding light on disulfide bond formation: engineering a redox switch in green fluorescent protein, *EMBO J. 20*, 5853−5862.
12. Miyawaki, A., Llopis, J., Heim, R., McCaffery, J. M., Adams, J. A., Ikura, M., and Tsien, R. Y. (1997) Fluorescent indicators for Ca2+ based on green fluorescent proteins and calmodulin, *Nature 388*, 882−887.
13. Barondeau, D. P., Kassmann, C. J., Tainer, J. A., and Getzoff, E. D. (2002) Structural chemistry of a green fluorescent protein Zn biosensor, *J. Am. Chem. Soc. 124*, 3522−3524.
14. Richmond, T. A., Takahashi, T. T., Shimkhada, R., and Bernsdorf, J. (2000) Engineered metal binding sites on green fluorescence protein, *Biochem. Biophys. Res. Commun. 268*, 462−465.
15. Wachter, R. M., Yarbrough, D., Kallio, K., and Remington, S. J. (2000) Crystallographic and energetic analysis of binding of selected anions to the yellow variants of green fluorescent protein, *J. Mol. Biol. 301*, 157−171.
16. Griesbeck, O., Baird, G. S., Campbell, R. E., Zacharias, D. A., and Tsien, R. Y. (2001) Reducing the environmental sensitivity of yellow fluorescent protein. Mechanism and applications, *J. Biol. Chem. 276*, 29188−29194.
17. Rekas, A., Alattia, J. R., Nagai, T., Miyawaki, A., and Ikura, M. (2002) Crystal structure of Venus, a yellow fluorescent protein with improved maturation and reduced environmental sensitivity, *J. Biol. Chem. 277*, 50573−50578.
18. McAnaney, T. B., Park, E. S., Hanson, G. T., Remington, S. J., and Boxer, S. G. (2002) Green fluorescent protein variants as ratiometric dual emission pH sensors. 2. Excited-state dynamics, *Biochemistry 41*, 15489−15494.
19. Chattoraj, M., King, B. A., Bublitz, G. U., and Boxer, S. G. (1996) Ultra-fast excited-state dynamics in green fluorescent protein: multiple states and proton transfer, *Proc. Natl. Acad. Sci. U.S.A. 93*, 8362−8367.
20. Yang, T. T., Sinai, P., Green, G., Kitts, P. A., Chen, Y. T., Lybarger, L., Chervenak, R., Patterson, G. H., Piston, D. W., and Kain, S. R. (1998) Improved fluorescence and dual color detection with enhanced blue and green variants of the green fluorescent protein, *J. Biol. Chem. 273*, 8212−8216.
21. Rizzo, M. A., Springer, G. H., Granada, B., and Piston, D. W. (2004) An improved cyan fluorescent protein variant useful for FRET, *Nat. Biotechnol. 22*, 445−449.
22. Glasoe, P. K., and Long, F. A. (1960) Use of glass electrodes to measure acidities in deuterium oxide, *J. Phys. Chem. 64*, 188−190.
23. Gardecki, J. A., and Maroncelli, M. (1998) Set of secondary emission standards for calibration of the spectral responsivity in emission spectroscopy, *Appl. Spectrosc. 52*, 1179−1189.
24. Weber, G., and Teale, F. W. J. (1957) Determination of the absolute quantum yield of fluorescent solutions, *Trans. Faraday Soc. 53*, 646−655.
25. Washburn, E. W. (2003) *International Critical Tables of Numerical Data, Physics, Chemistry and Technology*, 1st electronic ed., Vol. 7, Knovel, Norwich, NY.
26. Stanley, R. J., and Boxer, S. G. (1995) Oscillations in the spontaneous fluorescence from photosynthetic reaction centers, *J. Phys. Chem. 99*, 859−863.
27. Gustavsson, T., Cassara, L., Gulbinas, V., Gurzadyan, G., Mialocq, J. C., Pommeret, S., Sorgius, M., and van der Meulen, P. (1998) Femtosecond spectroscopic study of relaxation processes of three amino-substituted coumarin dyes in methanol and dimethyl sulfoxide, *J. Phys. Chem. A 102*, 4229−4245.
28. Naghibi, H., Tamura, A., and Sturtevant, J. M. (1995) Significant discrepancies between van't Hoff and calorimetric enthalpies, *Proc. Natl. Acad. Sci. U.S.A. 92*, 5597−5599.
29. Liu, Y. F., and Sturtevant, J. M. (1995) Significant discrepancies between van't Hoff and calorimetric enthalpies: II, *Protein Sci. 4*, 2559−2561.
30. Grynkiewicz, G., Poenie, M., and Tsien, R. Y. (1985) A new generation of Ca^{2+} indicators with greatly improved fluorescence properties, *J. Biol. Chem. 260*, 3440−3450.

31. Creemers, T. M. H., Lock, A. J., Subramaniam, V., Jovin, T. M., and Volker, S. (1999) Three photoconvertible forms of green fluorescent protein identified by spectral hole-burning, *Nat. Struct. Biol. 6*, 557−560.
32. Creemers, T. M. H., Lock, A. J., Subramaniam, V., Jovin, T. M., and Volker, S. (2000) Photophysics and optical switching in green fluorescent protein mutants, *Proc. Natl. Acad. Sci. U.S.A. 97*, 2974−2978.
33. Seebacher, C., Deeg, F. W., Brauchle, C., Wiehler, J., and Steipe, B. (1999) Stable low-temperature photoproducts and hole burning of green fluorescent protein (GFP), *J. Phys. Chem. B 103*, 7728−7732.
34. Wiehler, J., Jung, G., Seebacher, C., Zumbusch, Z., and Steipe, B. (2003) Mutagenic stabilization of the photocycle intermediate of green fluorescent protein (GFP), *ChemBioChem 4*, 1164−1171.
35. Litvinenko, K. L., Webber, N. M., and Meech, S. R. (2003) Internal conversion in the chromophore of the green fluorescent protein: temperature dependence and isoviscosity analysis, *J. Phys. Chem. A 107*, 2616−2623.
36. Webber, N. M., Litvinenko, K. L., and Meech, S. R. (2001) Radiationless relaxation in a synthetic analogue of the green fluorescent protein chromophore, *J. Phys. Chem. B 105*, 8036−8039.
37. Follenius-Wund, A., Bourotte, M., Schmitt, M., Iyice, F., Lami, H., Bourguignon, J. J., Haiech, J., and Pigault, C. (2003) Fluorescent derivatives of the GFP chromophore give a new insight into the GFP fluorescence process, *Biophys. J. 85*, 1839−1850.
38. Kummer, A. D., Kompa, C., Niwa, H., Hirano, T., Kojima, S., and Michel-Beyerle, M. E. (2002) Viscosity-dependent fluorescence decay of the GFP chromophore in solution due to fast internal conversion, *J. Phys. Chem. B 106*, 7554−7559.
39. Kummer, A. D., Wiehler, J., Schuttrigkeit, T. A., Berger, B. W., Steipe, B., and Michel-Beyerle, M. E. (2002) Picosecond time-resolved fluorescence from blue-emitting chromophore variants Y66F and Y66H of the green fluorescent protein, *ChemBioChem 3*, 659−663.

BI050132A